Published in final edited form as:
Neurobiol Dis. 2015 January ; 73: 106–117. doi:10.1016/j.nbd.2014.09.017.

Genetic Background Modulates Impaired Excitability of Inhibitory Neurons in a Mouse Model of Dravet Syndrome

Moran Rubinstein, **Ruth E. Westenbroek**, **Frank H. Yu**, **Christina J. Jones**, **Todd Scheuer**, and **William A. Catterall**
Department of Pharmacology, University of Washington, Seattle, WA 98195-7280

Abstract

Dominant loss-of-function mutations in voltage-gated sodium channel $Na_V1.1$ cause Dravet Syndrome, an intractable childhood-onset epilepsy. $Na_V1.1^{+/-}$ Dravet Syndrome mice in C57BL/6 genetic background exhibit severe seizures, cognitive and social impairments, and premature death. Here we show that Dravet Syndrome mice in pure 129/SvJ genetic background have many fewer seizures and much less premature death than in pure C57BL/6 background. These mice also have a higher threshold for thermally induced seizures, fewer myoclonic seizures, and no cognitive impairment, similar to patients with Genetic Epilepsy with Febrile Seizures Plus. Consistent with this mild phenotype, mutation of $Na_V1.1$ channels has much less physiological effect on neuronal excitability in 129/SvJ mice. In hippocampal slices, the excitability of CA1 Stratum Oriens interneurons is selectively impaired, while the excitability of CA1 pyramidal cells is unaffected. $Na_V1.1$ haploinsufficiency results in increased rheobase and threshold for action potential firing and impaired ability to sustain high-frequency firing. Moreover, deletion of $Na_V1.1$ markedly reduces the amplification and integration of synaptic events, further contributing to reduced excitability of interneurons. Excitability is less impaired in inhibitory neurons of Dravet Syndrome mice in 129/SvJ genetic background. Because specific deletion of $Na_V1.1$ in forebrain GABAergic interneuons is sufficient to cause the symptoms of Dravet Syndrome in mice, our results support the conclusion that the milder phenotype in 129/SvJ mice is caused by lesser impairment of sodium channel function and electrical excitability in their forebrain interneurons. This mild impairment of excitability of interneurons leads to a milder disease phenotype in 129/SvJ mice, similar to Genetic Epilepsy with Febrile Seizures Plus in humans.

Keywords

Dravet Syndrome; sodium channels; epilepsy; $Na_V1.1$; interneuron; Action potential threshold; Excitatory post synaptic potential amplification

Correspondence to: William A. Catterall. PhD., University of Washington, School of Medicine, Department of Pharmacology, Box 357280, Seattle, WA 98195-7280, USA, wcatt@uw.edu, Office: 206.543.1925, Fax: 206.543.3882.

Introduction

Voltage-gated sodium channels (Na_V) regulate neuronal excitability by initiation and propagation of action potentials and amplification of subthreshold synaptic events. Four pore-forming Na_V α subunits are primarily expressed in adult mammalian brain: $Na_V1.1$, $Na_V1.2$, $Na_V1.3$, and $Na_V1.6$, encoded by the *SCN1A, SCN2A, SCN3A*, and *SCN8A* genes, respectively. Mutations in *SCN1A* are the leading cause for a wide range of genetic epilepsies (Harkin et al., 2007), all involving infantile onset of febrile seizures that proceed beyond childhood. Missense mutations in *SCN1A* commonly lead to Genetic Epilepsy with Febrile Seizures Plus (GEFS+), a mild dominantly inherited epilepsy, with febrile and afebrile seizures that are well controlled by anti-epileptic drugs (Gambardella and Marini, 2009; Scheffer et al., 2009). Truncation mutations and other severe loss-of-function mutations cause Dravet Syndrome (DS, also called Severe Myoclonic Epilepsy of Infancy), a rare, genetically dominant, intractable convulsive disorder that begins during the first year of life, with seizures often associated with fever, and progresses to prolonged refractory seizures and frequent episodes of status epilepticus. During and after the second year of life, patients develop psychomotor delay, ataxia, cognitive impairment, and social interaction deficits (Genton et al., 2011; Li et al., 2011). Eighty percent of the identified mutations in DS arise de novo; however, ten to twenty percent of DS cases are inherited from mildly affected or unaffected parents (Claes et al., 2003; Claes et al., 2001; Depienne et al., 2010; Suls et al., 2010). Individual patients with apparently complete loss-of-function mutations demonstrate a broad range of disease severity and a wide-ranging combination of symptoms, suggesting that genetic background can strongly influence the severity and clinical presentation of DS (Dravet et al., 2005).

Mouse models of DS ($Na_V1.1^{+/-}$) (Ogiwara et al., 2007; Yu et al., 2006) demonstrated striking similarities to the human disease, with temperature- and age-dependent onset, and progression to myoclonic and generalized tonic-clonic seizures (Oakley et al., 2009). Genetic background can vastly affect seizure severity in mouse models and human patients (Frankel, 2009; Schauwecker, 2011). Accordingly, the severity of DS in mice has a striking dependence on genetic background. While DS mice in 129/SvJ (129) genetic background (DS/129) survive nearly as well as wild-type (WT) animals, eighty percent of DS mice in C57BL/6 (B6) genetic background (DS/B6) die by 12 weeks of age (Yu et al., 2006). Moreover, spontaneous seizures are rare in DS/129, whereas they are frequent in DS/B6 (Miller et al., 2013; Yu et al., 2006).

Functional studies of acutely dissociated hippocampal neurons from a DS mouse model demonstrated that loss of $Na_V1.1$ causes substantial reduction in sodium current density in GABAergic inhibitory interneurons without a corresponding change in sodium currents of excitatory pyramidal neurons (Yu et al., 2006). Similarly, cortical interneurons failed to sustain high frequency firing (Ogiwara et al., 2007). Moreover, specific deletion of $Na_V1.1$ in forebrain GABAergic interneurons leads to seizures and premature death (Cheah et al., 2012). Thus, disinhibition caused by selectively impaired excitability of GABAergic neurons is the underlying cause of epilepsy in DS mice. The availability of DS mouse strains with varying severity of disease provides an exceptional opportunity to examine the underlying physiological changes that are correlated with disease progression and severity.

Here we characterize the role of $Na_V1.1$ channels in interneuron excitability, emphasizing their role in setting threshold and rheobase, sustaining high-frequency trains of action potentials, and increasing amplitude and duration of subthreshold synaptic depolarizations. We show that these sodium channel functions are compromised in DS mice and contribute to reduced excitability in GABAergic inhibitory interneurons in the hippocampus. The degree of deficit differs in DS mice in the B6 and 129 genetic backgrounds, and is closely correlated with the severity of their disease symptoms. Because specific deletion of $Na_V1.1$ in forebrain GABAergic interneuons is sufficient to cause the symptoms of Dravet Syndrome in mice (Cheah et al., 2012), our results support the conclusion that the milder phenotype in 129/SvJ mice results from less impairment of sodium channel function and cellular excitability in GABAergic interneurons in forebrain neural circuits.

Our results show that differential reduction in excitability of GABAergic inhibitory interneurons is a key mechanism underlying genetic background effects in DS mice, and suggest that genotype-phenotype relationship in $Na_V1.1$ related epilepsies correlates with a spectrum of reduced excitability of interneurons (Catterall et al., 2010).

Materials and methods

Mice

Scn1a mutant mice were generated by targeted deletion of the last encoding exon as described previously (Yu et al., 2006). Mutant mice were generated on a 129×1/SvJ and kept on that background for at least 25 generations or backcrossed to C57BL/6J background for at least 20 generations. All experiments were performed according to guidelines established in the National Institutes of Health Guide for Care and Use of Laboratory Animals and were approved by the University of Washington Institutional Animal Care and Use Committee.

Thermal induction of seizures

Thermal induction of seizures was performed as described previously (Oakley et al., 2013; Oakley et al., 2009). Body temperature was measured continuously with a rectal temperature probe and controlled to ± 0.3 °C with a feedback temperature controller (TCAT2DF; Physitemp, Clifton, NJ) and heat lamp. Mouse body temperature was held at 37.0 °C for 10 min and then elevated by 0.5 °C every 2 min until a generalized tonic-clonic seizure (GTC) occurred or a body temperature of 42 °C was reached. For each mouse, the time and body temperature of each myoclonic or GTC seizure were determined from video recordings.

EEG recording

P25-P28 mice underwent survival surgery for implantation of EEG electrodes as described (Kalume et al., 2013). The mice were anesthetized with ketamine/xylazine (130/8.8 mg/kg). Using aseptic technique, a midline incision was made anterior to posterior to expose the cranium. Fine platinum wires were placed through small cranial holes created with a fine cutting needle and fixed in place with cyanoacrylite glue. Recording electrodes were placed at visually identified bilateral central locations. A reference electrode was placed at the midline cerebellum and a ground electrode was placed subcutaneously in the back. Electrode

impedances were typically <25 kΩ. After electrode placement, the skin was closed with suture and the mice were allowed to recover overnight.

Behavioral tests

The mice used for all behavioral analyses were 2–6 month-old adult males, and tests were performed as described previously (Han et al., 2012a).

Three-chamber social preference test

The three-chamber apparatus is an opaque plexiglass box (25 × 50 cm) with two transparent partitions that make left, center, and right chambers (25 × 16.7 cm). Each partition has a square opening (5 × 5 cm) in the bottom center. A cylindrical wire cage (10.5 cm diameter; Galaxy Pencil Cup, Spectrum Diversified Designs) was used as an inanimate object or as a cage housing a stranger mouse. A cylindrical bottle filled with water was placed on the top of the wire cup to prevent the test mouse from climbing to the top of the cup. The three chamber unit and wire cups were cleaned with 70% ethanol and wiped with paper towels between each trial. In the first 10-min habituation session, a test mouse was placed in the center of the three-chamber unit and was allowed to freely explore each chamber. In the second 10-min session, two wire cages were located in the left and right chambers. An age- and gender-matched WT/129 that had never been exposed to the test mouse, was placed in the right wire cage (mouse). The wire cage on the other side remained empty (object). Then, the test mouse was placed in the center, and allowed to freely explore the chamber for 10 min.

The movement of the mouse was recorded by a USB webcam (LifeCam HD-6000, Microsoft) and PC-based video capture software (WinAVI Video Capture, ZJMedia Digital Technology). The recorded video file was further analyzed by off-line video tracking software (EthoVision XT 7.0) to determine the time spent in each chamber.

Contextual fear-conditioning test

The contextual fear-conditioning chamber was a square arena (25 × 25 cm) with clear Plexiglas walls and a metal grid floor connected to a circuit board that delivered shocks to the metal grid (Coulbourn Instruments). An analog camera was attached on top of the chamber. The camera and the circuit board were connected to a personal computer, and its software (Freeze Frame 2.0, Actimetrics) controlled the circuit and recorded the data. The chamber was cleaned with 70% ethanol and wiped with paper towels before each session. In the habituation session, a test mouse was placed in the chamber and allowed to explore for 2 min. Immediately after habituation, the test mouse received a single mild foot shock (2 s, 0.5 mA). After one min, the mouse was removed from the chamber. For the 30-min and 24 h memory tests, the mouse was returned to the chamber (context) and its movement recorded for 2 min. The movement of mice was recorded by a USB webcam (LifeCam HD-6000, Microsoft) and PC-based video capture software (WinAVI Video Capture, ZJMedia Digital Technology). The recorded video file was further analyzed by off-line video tracking software (EthoVision XT 7.0).

Brain slice electrophysiology

Hippocampal slices were prepared from P21–P24 DS or WT littermate mice using standard procedures (Han et al., 2012a). Briefly, mice were deeply anesthetized with isoflurane and decapitated. The brain was quickly removed and hippocampal slices (300 μm) were cut with a modified Vibratome (Pelco 101 series 1000; Ted Pella, Inc., Redding, CA) in chilled (0–4°C) slicing solution containing 75 mM sucrose, 87 mM NaCl, 25 mM $NaHCO_3$, 25 mM D-glucose, 2.5 mM KCl, 1.25 mM NaH_2PO_4, 0.5 mM $CaCl_2$, 7.0 mM $MgCl_2$. The slices were transferred to a storage chamber with fresh ACSF containing 125 mM NaCl, 3 mM KCl, 2.0 mM $MgCl_2$, 2.0 mM $CaCl_2$, 1.25 mM NaH_2PO_4, 26 mM $NaHCO_3$, and 10 mM D-glucose, and incubated at 37 °C for 45 min. The slices were then incubated at room temperature for at least another 30 min before recording. All solutions were saturated with 95% O_2 and 5% CO_2. For the experiments described in Figures 3–5, coronal slices (300 μm thick) were used. In experiments described in Figure 6 and Figure 7 longitudinal slices were used to preserve most of the synaptic connections (Hajos and Mody, 1997; Tort et al., 2007). The brain was sagittally cut into two halves, and the hemispheres were glued on their callosal side onto a slope of 45° before slicing. Longitudinal sagittal slices (300 μm thick) were cut parallel to the axis of the hippocampus. Whole-cell current-clamp recordings were performed on *SO* CA1 interneurons or CA1 pyramidal neurons, visualized under differential interference contrast (DIC) optics, and near infrared (bandpass 750–800 nm) illumination was used to identify individual neurons in a recording chamber located on an upright microscope (Nikon Eclipse E600FW). Recordings were obtained through a Multiclamp 700A amplifier (Molecular Devices) by pCLAMP 8.0 software (Molecular Devices). Patch pipettes were filled with internal solution containing: 145 mM K-Gluconate, 2 mM $MgCl_2$, 0.5 mM EGTA, 2 mM ATP-Tris, 0.2 mM Na_2-GTP, 10 mM HEPES, pH to 7.2 with KOH. When filled with intracellular solution, patch electrode resistance ranged from 3 to 6 MΩ. Access resistance was monitored continuously for each cell. Only cells with access resistance less than 25 MΩ were recorded, and recordings were terminated/discarded when a significant (>10%) increase in access resistance occurred. Access resistance and capacitance were measured using the membrane test analysis tool in pClamp, and were similar among the different genotypes tested (Supplementary Table 1). The resting membrane potential was set to −60 mV by injection of no more than 50 pA, ranging from −50 to +50 pA, and was not affected by the DS mutation or genetic background (Supplementary Table 1). Bridge balance and pipette capacitance neutralization based on the amplifier circuit were applied to all current clamp recordings. Successful AP (%) (Figs. 3 and 5) was measured as the % of successful AP in response to 10 ms long depolarizing current step that was repeated 75 times at 1, 10 and 50 Hz. 100% indicates a successful AP in every trial, more than 100% indicate 2 AP for each depolarization (which only occurred with very strong depolarization). For experiments described in Figure 6, 5–10 mM QX-314 (Alomone Labs) was added to the internal solution. The stimulating electrode was placed on the alveus and the stimulation strength was carefully set to induce a depolarization of about 8 mV with less than 3 trials (each trial was 5 stimulations at 1 Hz). In order to completely block sodium channels, cells were voltage-clamped with repetitive depolarizations to 0 mV or +30 mV for 10–30 min until no inward current was observed during depolarizations. For the experiments described in Figure 7, the stimulating electrode was placed on the alveus and stimulation strength was set to produce firing probability of 50% during trains of stimuli (i.e., 5 AP out of 10 stimuli

delivered to the alveus at 1 Hz). For analysis, we included cells that fire 3–8 AP in response to 10 stimuli. Data from electrophysiology experiments were analyzed using Clampfit 9.0 (Molecular Devices) and Igor Pro (WaveMetrics) AP threshold was defined as 10 mV/ms, AP amplitude was measured between the AP threshold and peak.

Acute dissociation of hippocampal neurons

Hippocampal neurons were acutely isolated from P14-P16 and P21-P24 mice using standard procedures (Kalume et al., 2007). In brief, mice were deeply anesthetized with isoflurane and decapitated. The brain was quickly removed from the skull and submerged in an ice-cold dissection solution composed of 82 mM Na_2SO_4, 30 mM K_2SO_4, 5 mM $MgCl_2$, 10 mM HEPES, 10 mM D-glucose, 0.001% phenol red, at pH 7.4 and bubbled with 95% O_2/5% CO_2. 400 μM thick coronal slices of the brain were prepared and stored at room temperature for at least 1 h in a holding chamber containing a solution composed of 126 mM NaCl, 2.5 mM KCl, 2 mM $MgCl_2$, 2 mM $CaCl_2$, 1.25 mM NaH_2PO_4, 26 mM $NaHCO_3$, 10 mM glucose, 1 mM pyruvic acid, and saturated with 95% O_2/5% CO_2. Slices were transferred from the holding to the enzyme chamber, treated with 1.5 mg/ml protease type XIV (Sigma), and rinsed in dissection solution containing trypsin inhibitor (1 mg/ml) and bovine serum albumin (1 mg/ml). To isolate the neurons, the hippocampus was separated, cut into small chunks, and triturated with a fire-polished pipette in Tyrode's solution composed of 150 mM NaCl, 4 mM KCl, 2 mM $CaCl_2$, 2 $MgCl_2$, 10 HEPES, 10 glucose, at pH 7.4. Dissociated cells were plated on a poly-D-lysine-coated coverslip on the bottom of a 35 mm dish and allowed to settle for at least 15 min before recording. Whole-cell patch-clamp recordings were carried out at room temperature using an Axopatch 200B amplifier (Molecular Devices) and Pulse software (HEKA Electronics). Recording glass pipettes had resistances of 2–4 MΩ. Capacitative currents were minimized using the amplifier circuitry. We routinely used 80% series resistance compensation. The remaining linear capacity and leakage currents were eliminated by P/4 subtraction. The intracellular solution contained 160 mM N-methyl-D-glucamine, 40 mM HEPES, 4 mM $MgCl_2$, 10 mM EGTA, 1 mM NaCl, 14 mM phosphocreatine-Tris, 2 mM ATP-Tris, 0.2 mM Na_2GTP and 0.1 mM leupeptin, adjusted to pH 7.2 with H_2SO_4. The extracellular solution contained 20 mM NaCl, 116 mM glucose, 10 mM HEPES, 1 mM $BaCl_2$, 2 mM $MgCl_2$, 55 mM $CsCl_2$, 1 mM $CdCl_2$, 1 mM $CaCl_2$ and 20 mM tetraethylammonium chloride, adjusted to pH 7.35 with NaOH. The voltage dependence of activation was measured from a holding potential of −85 mV. Cells were depolarized to potentials from −70 to +30 mV in 5-mV increments, and peak inward currents were measured. Conductance (G)-voltage relationships were determined from peak current (I) versus voltage relationships as $G = I/(V - V_{Rev})$, where V was the test potential, and V_{Rev} was the extrapolated reversal potential. The voltage dependence of inactivation was measured from a holding potential of −100 mV. Cells were depolarized for 100 ms to potentials from −100 to +20 mV in 5-mV increments followed by test pulses to −20 mV. Data were analyzed using Igor Pro (WaveMetrics).

Statistics

Data are reported as mean ± SE. Comparisons within groups were done by one-way ANOVA or Student’s t-test as appropriate. Differences were considered significant at $p < 0.05$.

Results

The epileptic phenotype in DS/129 mice

For most DS patients, the first sign of disease is a febrile seizure, occurring between 6–9 months of age, followed by progression to febrile and afebrile seizures, including tonic–clonic, myoclonic, and absence forms that are refractory to current therapies (Dravet et al., 2005; Genton et al., 2011). Similarly DS/B6 mice develop normally until their fourth week of life, when they start to experience frequent spontaneous seizures, and often succumb to premature death (Kalume et al., 2013; Oakley et al., 2009; Yu et al., 2006). In contrast, DS/129 mice survive similarly to WT mice (Miller et al., 2013; Yu et al., 2006), and no signs of behavioral seizures were detected in video recordings from P21-P28.

DS/B6 mice are highly susceptible to thermally induced seizures (Oakley et al., 2009). Therefore we determined whether DS/129 mice were also susceptible to seizures in response to elevated temperature, despite their lack of spontaneous behavioral seizures or premature deaths. At P21, elevated temperature was sufficient to induce generalized tonic-clonic (GTC) seizures in both genetic backgrounds (Fig. 1A, C and (Oakley et al., 2009)), but with different sensitivity. Similar to DS patients (Verbeek et al., 2013), DS/B6 mice had thermally induced GTC seizures below 38.5 °C, with a mean temperature for seizure induction of 37.9 ± 0.3°C (Fig. 1A). In contrast, no DS/129 mice had GTC seizures below 38.5 °C, but all had GTCs at higher temperatures, with an average of 39.1 ± 0.2 °C (Fig. 1A). Another striking difference between the genetic backgrounds became evident through analysis of myoclonic seizures. This type of seizure is characteristic in DS, but is less common in milder forms of *SCN1A*-associated epilepsies such as GEFS+ (Gambardella and Marini, 2009). Similar to DS patients, all DS/B6 mice had myoclonic seizures preceding their thermally induced GTC seizure (Fig. 1B (Oakley et al., 2013)). In contrast, 30% of DS/129 mice did not have myoclonic seizures (Fig. 1B). Thus, in parallel with their lesser susceptibility to spontaneous death, seizure phenotype is much less severe in DS/129 mice than it is in DS/B6.

Since mental retardation and cognitive impairment are observed in most DS patients (Buoni et al., 2006; Guzzetta, 2011), we compared the cognitive and social abilities of DS/B6 and DS/129 mice. DS/B6 mice were shown previously to have deficits in spatial memory (Han et al., 2012a). In contrast, DS/129 mice did not show impaired context-dependent fear memory, and their performance was indistinguishable from WT/129 (Fig. 1D). Mutations in *SCN1A* are also linked to social deficits in idiopathic autism, GEFS+, and DS (Li et al., 2011; Mahoney et al., 2009; Weiss et al., 2003), and DS/B6 mice exhibited social interaction deficits when tested in the three-chamber paradigm (Han et al., 2012a). Likewise, DS/129 mice also had social interaction deficits (Fig. 1E). Whereas WT/129 mice spent far more time interacting with a stranger mouse than with an inanimate object, DS/129 mice did not show a significant preference (Fig. 1E). Together, these pathophysiological and behavioral data demonstrate that genetic background can vastly affect the outcome of an identical truncation mutation in mouse models of DS. While DS/B6 mice are an exceptionally good phenocopy of human DS, the milder epilepsy, lower number of myoclonic seizures, and lack

of cognitive deficit in DS/129 mice are more consistent with the milder clinical manifestations of human GEFS+ (see Discussion).

Differential loss of excitability in hippocampal interneurons correlated with severity of epilepsy

Previous in-vitro examination of Na_V channel function and expression was performed on DS mice of mixed B6 and 129 (50:50) or DS/129 genetic background (Mistry et al., 2014; Ogiwara et al., 2007; Yu et al., 2006). To more fully assess the effect of genetic background, we recorded sodium currents from acutely dissociated hippocampal interneurons from WT and DS neurons from mice of the two pure genetic backgrounds using whole-cell voltage clamp. GABAergic inhibitory neurons were identified by cell morphology (Yu et al., 2006). We hypothesized that the degree of reduction in somatic sodium currents would correlate with the severity of epilepsy in DS/B6 and DS/129 mice. We first measured somatic sodium currents at P14, an age at which mice of mixed genetic background have reduced sodium currents (Yu et al., 2006). At P14, sodium currents were reduced by ~50% in DS/B6 mice, while currents of DS/129 were not different from WT/129 (Figs. 2A–C). Despite the differences in current amplitude, no changes in the voltage dependence of activation or inactivation were observed (Fig. 2D). Thus, at P14, the severely affected DS/B6 display a marked reduction in sodium currents as was observed in mice of mixed background, while sodium currents are preserved in DS/129, in correlation with the milder epilepsy phenotype. We then made similar measurements at P21, the age at which DS/B6 mice have generalized tonic clonic seizures. Surprisingly, cell-body sodium currents densities were similar across all strains and genotypes (Figs. 2E, F), as were the voltage dependence of activation or inactivation (Fig. 2G). The basis for the lack of differences in sodium current density in the cell soma among genotypes at P21 is unknown. Na_V channels are localized throughout the neuron, and their presence in dendrites, cell body, and axon initial segment is critical for normal firing (Bean, 2007). It is possible that the localization of $Na_V1.1$ is changed, such that the channel density is similar among the genotypes in the cell soma but is different in dendrites or axon initial segments. Alternatively, it is possible that mutant $Na_V1.1$ channels are replaced by other sodium channel subtypes in both strains of DS mice, but this up-regulation is unable to fully compensate for loss of $Na_V1.1$ because of differences in localization or functional properties.

Therefore, to examine cellular excitability in the context of intact cellular architecture, we studied excitability of pyramidal neurons and GABAergic interneurons in hippocampal slices, in which cellular morphology and circuit properties are preserved. AP firing properties of individual excitatory and inhibitory neurons were examined using depolarizing current injection into the cell soma in whole-cell current clamp configuration.

Deletion of Na_V 1.1 had no effect on firing of CA1 pyramidal cells of either DS/B6 or DS/129 mice (Fig. 3). We did not detect any difference in AP rheobase, threshold (Figs. 3A, B), or average firing frequency in response to 1 s of depolarizing current injection (Fig. 3C). We also tested AP firing in response to a short (10 ms) depolarizing current injection that was repeated 75 times at 1, 10, and 50 Hz. In this protocol, depolarizations are transient and an AP will be evoked only if threshold is reached before the end of the pulse. The percent of

successful AP generation in trains of stimuli was similar between WT and DS animals of both strains (Figs. 3D–F; 100% indicates one successful AP in every trial; more than 100% indicates that 2 APs were sometimes evoked during the 10 ms depolarization). These data are consistent with the view that disinhibition caused by loss of function in interneurons, and not hyperexcitability of pyramidal cells, is the neuronal basis of epilepsy in DS mice (Cheah et al., 2012; Ogiwara et al., 2013; Ogiwara et al., 2007; Yu et al., 2006).

Despite the lack of effect of DS mutations, B6 and 129 pyramidal neurons differed in excitability. The rheobase for AP generation in CA1 pyramidal neurons was lower in 129 animals compared to B6 animals, regardless of the DS mutation (Fig. 3B and Table 1). In addition, at each level of current injection, more APs were generated in 129 than in B6 mice (Figs. 3C–F). This demonstrates that genetic background can modify intrinsic excitability of neurons and does modify excitability of CA1 pyramidal neurons.

In order to compare the effects of the DS mutation on a specific class of inhibitory interneurons, we examined the excitability and function of CA1 Stratum Oriens (*SO*) interneurons. Horizontal *SO* interneurons are activated by recurrent collaterals of pyramidal cells and mediate feedback inhibition of neighboring pyramidal cells (Blasco-Ibanez and Freund, 1995; Klausberger and Somogyi, 2008; Pouille and Scanziani, 2004). Furthermore, activation of *SO* interneurons regulates the strength of depolarization of CA1 principal cells by the temporoammonic pathway (Coulter et al., 2011; Maccaferri and McBain, 1995). Thus, *SO* interneurons are key modulators of the activity of CA1 pyramidal cells and thereby control the final output of the hippocampus to extra-hippocampal regions. Consistent with this role, dysfunction of *SO* interneurons has been implicated in facilitation of seizures in temporal lobe epilepsy (Ang et al., 2006).

Injection of depolarizing current in whole-cell configuration induced APs in *SO* interneurons of all four genotypes (Fig. 4A). The threshold for AP generation in *SO* interneurons was lower in both WT/129 and DS/129 compared to WT/B6 and DS/B6 (Fig. 4B), indicating that genetic background substantially alters neuronal excitability of *SO* interneurons. The rheobase for AP generation was similar in WT/129, WT/B6, and DS/129 mice, but higher in DS/B6 mice (Fig. 4C), suggesting that the excitability of DS/129 is better maintained than that of DS/B6. In addition, DS/B6 animals had more substantially reduced AP amplitude and maximal rate of rise than DS/129, consistent with reduced sodium conductance during AP firing (Figs. 4D, E).

To further explore the changes in AP generation caused by the differences in threshold and rheobase, we measured the probability of AP firing in response to short, repetitive injection of depolarizing current at 1, 10, and 50 Hz. Notably, the firing of DS/B6 was reduced at all tested frequencies, especially near rheobase. In contrast, AP firing of DS/129 was less strongly reduced compared to WT/129 (Figs. 5A–C). At the 200 pA stimulus level, firing of DS/B6 was significantly more reduced at each tested frequency than DS/129 (Fig. 5D). O-LM cells are likely to represent a large proportion (80–100%) of *SO* horizontal neurons in hippocampal slices (Ali and Thomson, 1998; Pouille and Scanziani, 2004). In our hands, all cells that were successfully filled with biocytin and reconstructed (14 of 21 neurons), displayed the characteristic morphology (Maccaferri, 2005) and firing of O-LM cells

(Supplementary Fig. 1). As these interneurons usually fire at theta frequencies (5–10 Hz) (Klausberger et al., 2003; Maccaferri, 2005; Maccaferri and McBain, 1996), the reduced ability of DS/B6 interneurons to fire an AP in response to stimulus intensities up to 250 pA, in this frequency range, suggests significant impairment of their normal physiological function (Figs. 5B, D). Together, these data demonstrate that DS/B6 have a physiologically significant reduction in AP firing capability due to increased rheobase and threshold, and reduced sodium conductance, and these reductions in excitability of DS/B6 *SO* interneurons are more substantial than for DS/129 mice.

Amplification of subthreshold synaptic events by sodium current in Stratum Oriens interneurons

In excitatory cortical and hippocampal neurons, transient and persistent sodium currents activate at subthreshold voltages and enhance the postsynaptic response to excitatory events in dendrites and cell soma (Carter et al., 2012; Fricker and Miles, 2000; Schwindt and Crill, 1995; Stuart and Sakmann, 1995). Moreover, the localization of $Na_V1.1$ to the cell soma (Westenbroek et al., 1989) suggests that this sodium channel subtype might have a specific role in amplification and integration of excitatory postsynaptic potentials (EPSPs). To test whether loss of $Na_V1.1$ channels in the DS mice affects amplification of synaptic inputs in CA1 *SO* interneurons, a stimulating electrode was placed in the alveus to activate the axons of CA1 pyramidal cells antidromically (Maccaferri and McBain, 1995; Pouille and Scanziani, 2004), and the resulting EPSPs were recorded in *SO* interneurons using the whole-cell configuration in current-clamp mode. The stimulation intensity was set to evoke a subthreshold EPSP depolarization of ~ 8 mV in all genotypes (Figs. 6A, B), effectively normalizing for their differences in excitability. After amplitude normalization, EPSP duration (Fig. 6C) and EPSP time integral (Fig. 6D) were similar for WT/B6, DS/B6 and DS/129 (open bars). Interestingly, WT/129 mice had EPSPs that were prolonged compared to the other genotypes (Figs. 6A, C, D). However, EPSP shape was not substantially different between DS/129, DS/B6 and WT/B6 animals. Thus, EPSP kinetics *per se* are not likely to contribute to the disease phenotype.

In order to examine the contribution of Na_V channels to the 8-mV EPSPs at this inhibitory synapse, we added QX-314 to the intracellular solution to serve as a membrane-impermeant open-channel blocker of Na_V channels (Salazar et al., 1996). This allowed recording of EPSPs before and after block of Na_V channels by intracellular diffusion of the drug from the recording pipette into the cell. The results summarized in Fig. 6B–D demonstrate that sodium currents contribute substantially to EPSP amplitude, duration, and time integral of depolarization in *SO* interneurons in all genotypes (difference between open and filled bars, Figs. 6B–D), as previously observed for excitatory neurons. Evidently, Na_V channels are crucial for EPSP amplification in *SO* inhibitory neurons, and this function may be adversely affected by loss of $Na_V1.1$ channels in DS. To our knowledge, this is the first evidence for amplification of EPSPs by sodium channels in inhibitory interneurons.

In WT/B6 and WT/129 mice, Na_V channels made a similar contribution to the EPSP amplitude (Fig. 6B, 3.9 ± 0.6 mV reduction by QX-314 block in WT/129 vs. 3.6 ± 0.6 mV in WT/B6; p=0.75). In the mutant DS/B6 and DS/129 mice, the contribution of Na_V

channels to EPSP amplitude was greatly reduced, but the contribution of Na_V channels was similar between DS/B6 and DS/129 (Fig. 6B, 1.5 ± 0.6 mV reduction by QX-314 block in DS/129, and 1.1 ± 0.5 mV in DS/B6; $p>0.05$ vs. each other; $p<0.01$ vs. WT). These results indicate that $Na_V1.1$ channels make an important contribution to EPSP amplitude that is reduced in DS animals. However, that contribution does not differ greatly between 129 and B6 genotypes. This result suggests that an equivalent level of synaptic release of neurotransmitter would result in a substantially smaller EPSP in DS mice as a result of the reduction in EPSP boosting by $Na_V1.1$ channels.

The greater duration and time integral of depolarization during EPSPs in WT/129 were accompanied by a greater block of EPSP duration and time integral by QX-314 than we observed for WT/B6 (Figs. 6C, D). Nevertheless, block of Na_V channels had a similar fractional effect on half-width in both WT strains (Figs. 6C and E; WT/129 EPSP half width was reduced by 41.5 ± 8.6 % and WT/B6 by 39 ± 5 % after QX-314 block; $p=0.8$). Substantial differences in EPSP duration and time integral persist between WT/B6 and WT/129 after block by QX-314, suggesting that the longer EPSP and greater integral of depolarization in WT/129 may not be primarily attributable to Na_V channels, even though Na_V channels amplify those differences (Figs. 6C, D).

The effects of block of Na_V channels with QX-314 on EPSPs are directly compared in Figure 6E and F, which illustrates the percent reduction in EPSP duration and time integral caused by QX-314. The percentage reduction in EPSP duration and time integral by QX-314 was similar for WT/129 and WT/B6. However, Na_V channels contributed significantly less to EPSP duration and time integral in DS/B6 than in DS/129 (Figs. 6E, F). These results indicate that the percent contribution of Na_V channels to the time integral of depolarization during the EPSP was similar in WT/B6 and WT/129, but was significantly smaller in DS/B6 than in DS/129.

Altogether, sodium channels account for ~40% of the amplitude and ~60% of the time integral of depolarization of subthreshold EPSPs in *SO* interneurons (Figs. 6E, F). In DS/129 mice, despite deletion of $Na_V1.1$, the relative contribution of Na_V channels to EPSP amplification was similar to that of WT. In contrast, identical deletion of $Na_V1.1$ in the DS/B6 mice results in reduced amplification of EPSPs by sodium currents in *SO* interneurons (Figs. 6E, F).

Effects of mutation of $Na_V1.1$ channels on synaptically evoked APs

The contribution of $Na_V1.1$ to AP firing was further studied with higher levels of synaptic stimulation. The stimulating electrode was again placed in the alveus, but the stimulus intensity was set to produce a firing probability of 50% during trains of stimuli (i.e., 5 AP out of 10 stimuli delivered to the alveus at 1 Hz). This experimental approach effectively normalized for the differences among genotypes in sustaining trains of action potentials. The threshold for AP generation during these trains of stimuli with identical firing probability was similar for WT/129, WT/B6, and DS/B6. However, the threshold was hyperpolarized by ~4 mV in DS/129, suggesting increased excitability compared to DS/B6 (Figs. 7A, B). Moreover, while deletion of $Na_V1.1$ itself had no effect on spike amplitude of synaptically evoked APs, WT/129 mice showed lower spike amplitude compared to B6 (Fig. 7C),

indicating that genetic background, rather than $Na_V1.1$ deletion, governs this neuronal property when APs are evoked synaptically with stimuli set to normalize the firing probability.

We analyzed the physiological properties of these near-threshold EPSPs in *SO* interneurons. As deletion of $Na_V1.1$ had differential effects on the amplification of subthreshold EPSPs by sodium currents (Fig. 6), these differences should be augmented in near-threshold EPSPs because of the high voltage dependence of sodium channels (Carter et al., 2012). EPSPs were shorter in both DS strains compared to WT (Figs. 7E, J), with reduced time to peak (Fig 7I), which shortened the latency to AP generation (Fig. 7D). Variations in spike latency, and the resulting jitter, are important for coding information in neural circuits. Since APs are evoked from the rising phase or the plateau of the EPSP, spike latency and jitter are highly dependent on EPSP duration (Fricker and Miles, 2000; Vervaeke et al., 2006). Accordingly, EPSP shortening in DS neurons (Figs. 7E, J) caused reduced latency to spikes and reduced jitter in both strains (Figs. 7D, F, G). Thus, in both DS genotypes, there is a shorter and more consistent latency to AP firing during trains in which the overall probability of firing was normalized by the stimulus protocol.

Quantitative analysis of the physiological properties of the near-threshold EPSPs revealed important differences among genotypes. The amplitude of near-threshold EPSPs was similar among WT/129, WT/B6 and DS/B6, but smaller in DS/129 (Fig. 7H). This result is consistent with the more negative threshold at which APs are fired in DS/129 neurons (Fig. 7B). Deletion of $Na_V1.1$ resulted in ~50% shortening of near-threshold EPSPs in both DS strains (Figs. 7E, J), which was accompanied by a marked reduction in the time integral of depolarization (Fig. 7K). Despite the greatly reduced width and time integral in both DS genotypes, there was a marked strain-dependent difference in EPSP duration such that EPSPs in WT/129 were 50% longer compared to those in WT/B6 (Fig. 7I). Accordingly, the half-width of EPSPs in DS/129 was ~40% longer compared to DS/B6, and was increased toward the EPSP duration of WT/B6 (Fig. 7J). Longer lasting EPSPs allow better integration of subthreshold synaptic events and would contribute further to the increased excitability of DS/129 neurons and to the more effective preservation of excitability than DS/B6.

Discussion

Epileptic phenotype in DS/129 mice

SCN1A is the gene most frequently associated with epilepsy (Harkin et al., 2007), and mutations of differing severity in this gene are responsible for a wide range of genetic epilepsies from benign familial febrile seizures to intractable epilepsy (Catterall et al., 2010). To date, 41 of 42 *SCN1A* mutations found in GEFS+ patients are missense mutations that are expected to alter, but not abolish, $Na_V1.1$ function (Claes et al., 2009; Escayg and Goldin, 2010), while truncation mutations and other complete loss of function mutation are associated with DS (Claes et al., 2009). Thus, differences in phenotype can be greatly affected by the genetic mutation and its severity. However, as shown here, the genotype-phenotype relationship can also be greatly affected by genetic background. Deletion of $Na_V1.1$ in C57BL/6 mice recapitulates human DS with high fidelity. In a parallel sequence with disease progression in DS patients, our DS mice develop normally until the third

postnatal week when seizures can be induced by increased core body temperature. After P21, spontaneous seizures begin, premature death occurs frequently, and DS-associated comorbidities develop, including ataxia, circadian rhythm defects, cognitive deficits, and social impairments (Han et al., 2012a; Han et al., 2012b; Kalume et al., 2013; Kalume et al., 2007; Oakley et al., 2009; Yu et al., 2006). Conversely, the same gene deletion made in 129/SvJ genetic background has far lesser effects. 129/DS mice are rarely subject to spontaneous seizures nor do they die prematurely. Here we show that DS/129 require greater increases in core body temperature for thermal induction of seizures, and they have normal cognitive function in context-dependent fear conditioning in contrast to DS/B6 mice. These characteristic differences in disease severity, when an identical DS deletion mutation is introduced into C57BL/6 vs. 129/SvJ mice, provide an exceptional opportunity to probe the underlying pathophysiological basis for the strain-specific differences in neuronal function.

Overall, the less severe epileptic phenotype of DS/129 mice is more consistent with the milder phenotype of human GEFS+ patients than the more severe phenotype of most human DS patients. GEFS+ patients are less susceptible to myoclonic seizures than DS patients (Gambardella and Marini, 2009). Similarly, myoclonic seizures were less prevalent in DS/129 mice than in DS/B6 animals (Fig. 1B). No cognitive impairment is observed in human GEFS+ patients in parallel with the lack of deficit in context-dependent fear memory in DS/129 (Fig. 1D). Thus, the identical DS mutation expressed on the 129/SvJ background rather than the C57BL/6J background is sufficient to alter the epileptic phenotype almost as drastically as do the different genetic defects that lead to GEFS+ vs. DS.

Specific deletion of $Na_V1.1$ in forebrain GABAergic inhibitory neurons recapitulates all of the major symptoms of DS (Cheah et al., 2012; Han et al., 2012a; Ogiwara et al., 2013). Furthermore, we found no functional differences between the hippocampal CA1 pyramidal neurons of DS/B6 and DS/129 mice (Fig. 3 and Table 1). Therefore, the primary cause of DS is expected to be dysfunction of inhibitory neurons, which is the focus of this study.

Differences in neuronal excitability between WT/B6 and WT/129 mice

Mouse models are invaluable for understanding the molecular basis of human genetic diseases, as well as the molecular basis underlying differences in disease severity. For example, strain-dependent variation in sensitivity to kainic acid-induced seizures (McKhann et al., 2003), as well as performance in learning and memory tests, and synaptic plasticity (Nguyen, 2006; Schimanski and Nguyen, 2004), have been reported for C57BL/6 and 129 strains, arguing that background differences in neuronal function can affect complex phenotypes in these WT strains. Along this line, we found that neuronal function differed in the two WT strains. CA1 pyramidal neurons of WT/129 had lower rheobase (Fig. 3B and Table 1), and *SO* interneurons of WT/129 had lower threshold for AP generation compared to WT/B6 (Fig. 4B). Moreover, genetic background differences modulated the duration of EPSPs in *SO* neurons substantially (Figs. 6 and 7). All of these differences may contribute to the overall differential excitability profiles of WT/B6 and WT/129 mice.

Genetic background determines the impact of the DS mutation on cellular excitability

Previous studies of *Scn1a* mutant DS mice, and the data presented here, provide strong evidence that the molecular basis for DS is disinhibition. (i) DS epilepsy and its associated comorbidities could be replicated in mice with selective deletion of *Scn1a* in interneurons (Cheah et al., 2012; Han et al., 2012a; Ogiwara et al., 2013); (ii) Selective deletion of *Scn1a* in excitatory neurons had no effect or even reduced DS symptoms (Dutton et al., 2012; Ogiwara et al., 2013); and (iii) excitability of CA1 pyramidal neurons (Fig. 3 and Table 1) and layer 5 pyramidal neurons (Tai et al., 2014) was unaffected by the DS mutation. In contrast, a recent study of *Scn1b*-based model of DS, demonstrated hyperexcitability of subicular and layer 2/3 pyramidal neurons (Reid et al., 2014), indicating that ablation of different genes can dramatically alter the cellular basis and pathophysiological mechanisms of DS.

In contrast to pyramidal neurons, we show here that excitability is compromised in GABAergic interneurons of both strains but that the deficit is greater in C57BL/6 than in 129/SvJ. (i) Sodium currents in acutely dissociated GABAergic inhibitory neurons are reduced in DS/B6 but not in DS/129 at P14 (Fig. 2); (ii) DS/B6 show higher threshold and rheobase for AP firing, reduced AP amplitude, and reduced AP maximum rate of rise at P21 (Fig. 4), all consistent with reduced sodium conductance (Bean, 2007); and (iii) firing probability in response to depolarizing current injection was more severely reduced for DS/B6 compared to DS/129 mice at P21 (Fig. 5). Firing is dictated by a delicate balance of inward and outward ionic currents at subthreshold potentials. That balance controls the rate of subthreshold depolarization, which ultimately brings the membrane potential to threshold and results in neuronal firing. The firing deficit in DS/B6 suggests that $Na_V1.1$ is a particularly important contributor to this balance and strongly affects threshold in the C57BL/6 genetic background. After threshold is reached, all the available subtypes of brain Na_V channels are fully activated, and the sodium current conducted by $Na_V1.1$ plus other sodium channels is sufficient to support the action potential, even in the presence of the DS mutation. Remarkably, on P21 when spontaneous seizures are first observed, the excitability of *SO* interneurons in response to direct depolarization is substantially reduced in DS/B6, but only slightly affected in DS/129. These data demonstrate directly that DS/B6 mice have a physiologically significant reduction in AP firing capability, while excitability is better preserved in DS/129.

DS mice on a 50:50 129/SvJ:C57BL/6 background have an intermediate disease phenotype compared to the pure strains (Miller et al., 2013; Mistry et al., 2014; Yu et al., 2006). Electrophysiological studies of the cell bodies of dissociated neurons from the hippocampus show both a decrease of sodium current in interneurons and an increase in sodium current in pyramidal cells in 50:50 129/SvJ:C57BL/6 compared to pure 129/SvJ (Mistry et al., 2014). In contrast, we observe only a decrease in sodium current in interneurons at P14 when analyzed with similar methods and pure mouse strains in our experiments (Fig. 2). This difference in results may reflect the difference in genotypes. Moreover, as we show here, it is important to assess the effects of $Na_V1.1$ mutations on electrical excitability of intact neurons in brain slice preparations where they retain their dendrites and axon initial

segments because these subcellular compartments are crucial in integration and boosting incoming synaptic signals and in initiating action potentials.

$Na_V1.1$ contributes differentially to EPSP duration and amplification in C57BL/6 and 129/SvJ mice

Excitatory synaptic inputs from presynaptic neurons are integrated, amplified, and conducted along the dendrites and cell soma to the axon initial segment, the preferred site for AP generation. In addition to their critical role in AP firing, transient and persistent sodium currents combine to enhance and amplify the response to subthreshold synaptic inputs (Carter et al., 2012; Fricker and Miles, 2000; Martina et al., 2000; Schwindt and Crill, 1995; Stuart and Sakmann, 1995; Vervaeke et al., 2006). $Na_V1.1$, $Na_V1.2$, $Na_V1.3$ and $Na_V1.6$ were all shown to contribute to both transient and persistent sodium currents (Estacion et al., 2010; Kalume et al., 2007; Raman and Bean, 1997). In layer 5 pyramidal cells application of TTX reduced the time integral of EPSPs by ~70% (Gonzalez-Burgos and Barrionuevo, 2001; Rotaru et al., 2007; Stuart and Sakmann, 1995). In our experiments, QX-314 blocked 60% of the EPSP time integral in WT mice, and that block was reduced by 40–50% in DS mice (Fig. 6D, white bars). Moreover, deletion of $Na_V1.1$ resulted in ~60% reduction in the time integral of the near-threshold EPSP (Fig. 7K), indicating that $Na_V1.1$ currents accounts for a substantial portion of the sodium currents during EPSP. These effects suggest that $Na_V1.1$ serves a major role among different sodium channel subtypes in boosting EPSPs in *SO* interneurons.

DS/129 inhibitory neurons are substantially more likely to fire in response to synaptic depolarization than DS/B6. At least three characteristic differences contribute to this enhanced AP firing in response to EPSPs: (i) the loss of amplification of subthreshold EPSPs caused by deletion of $Na_V1.1$ channels was greater in DS/B6 (Figs. 6E, F), and is expected to be even greater at near-threshold EPSPs; (ii) DS/129 mice have ~4 mV more negative threshold for synaptically evoked APs (Figs. 7A, B); and (iii) the duration of the near-threshold EPSP was 40% longer in DS/129 compared to DS/B6, allowing better temporal summation of excitatory events (Figs. 7E, J). Together, these differences provide a plausible mechanism for the nearly normal firing properties observed in DS/129, and the reduced action potential firing and reduced inhibitory neurotransmission in DS/B6.

Overall contributions to reduced excitability of SO neurons

Our experiments show that the DS mutations impact excitability of interneurons in two ways. First, an equivalent amount of neurotransmitter release at synapses will result in far smaller EPSPs of shorter duration in *SO* interneurons of DS mice than of WT mice. The reduced amplitude and shorter time course of EPSPs combine to greatly reduce the time integral of postsynaptic depolarization and the probability of reaching threshold. Second, these effects on the efficacy of synaptic currents in depolarizing the postsynaptic neuron convolve with reduced excitability of the postsynaptic neuron as measured in experiments of Figs. 4 and 5 to reduce overall output of action potentials and inhibitory neurotransmission.

The strikingly greater deficit of excitability in DS/B6 compared to DS/129 interneurons is likely caused by greater deficiencies of DS/B6 neurons in both amplification of incoming

EPSPs and initiation of action potentials. The reduction in intrinsic excitability observed in the experiments of Figures 4 and 5 is clearly greater for DS/B6 than for DS/129. Moreover, for near threshold synaptic activation (Fig. 7), the threshold for activation is reduced in DS/129 relative to the other genotypes. These deficits sum up to a substantially greater impact of the DS mutation in DS/B6 mice than in DS/129 mice.

Role of the hippocampus in DS

The reduction of sodium currents, measured by whole-cell voltage clamp in dissociated hippocampal inhibitory neurons at P14, is approximately 50% in heterozygous DS mice, which is the expected maximum for mutation of one allele of the *Scn1a* gene (Fig. 2 and (Yu et al., 2006). However, previous studies of other classes of GABAergic inhibitory neurons from DS mice showed smaller reductions of sodium currents: 40% for Purkinje neurons in the cerebellum (Kalume et al., 2007) and <15% for GABAergic inhibitory interneurons in the cerebral cortex (Tai et al., 2014). As we have shown here, hippocampal GABAergic inhibitory neurons are impaired in AP generation at P21, the day of onset of epilepsy, and the impairment is greater in DS/B6, the more seriously affected mouse strain. These results suggest that the hippocampus might play a prominent role in DS. The dysfunction of interneurons in the hippocampus on P21 could be involved in epileptogenesis and/or in seizure generation itself. The generalized tonic-clonic seizures that are observed in our DS mice (Oakley et al., 2009; Yu et al., 2006) must be primarily generated in the cerebral cortex (Fig. 1), but it remains possible that they are initially driven by hippocampal hyperactivity that induces generalized seizure activity in the cerebral cortex within milliseconds (Liautard et al., 2013). Moreover, it is also possible that the hyperexcitability of the hippocampus serves to kindle the development of epilepsy by permanently altering electrical excitability in both hippocampus and cerebral cortex. The reduced hippocampal hyperexcitability in DS/129 mice, resulting from relatively greater excitability of GABAergic interneurons, would provide a weaker stimulus for seizure initiation, consistent with the smaller number of myoclonic seizures we observe before initiation of a generalized tonic-clonic seizures in DS/129 mice (Fig. 1). This weaker stimulus for hyperactivity of the cerebral cortex may result in lower frequency and reduced severity of seizures in DS/129 mice. More detailed in vivo electrophysiological recordings with high-resolution depth electrodes will be required to define the site where seizures are initiated and further assess the contribution of hyperactivity in the hippocampus to this process.

Conclusions

Increasing severity of loss-of-function mutations of $Na_V1.1$ channels causes progressively more severe epilepsy syndromes, from familial febrile seizures to GEFS+ and finally DS (Catterall et al., 2010). We show here that the genotype-phenotype relationship can also be greatly affected by genetic background, and demonstrate that the degree of loss of excitability in GABAergic interneurons correlates with the severity of the epileptic phenotype in DS/B6 and DS/129 mice.

Supplementary Material

Refer to Web version on PubMed Central for supplementary material.

Acknowledgments

Research reported in this publication was supported by the National Institute of Neurological Disorders and Stroke of the National Institutes of Health under award number R01NS25704. The content is solely the responsibility of the authors and does not necessarily represent the official views of the National Institutes of Health.

References

Ali AB, Thomson AM. Facilitating pyramid to horizontal oriens-alveus interneurone inputs: dual intracellular recordings in slices of rat hippocampus. J Physiol. 1998; 507(Pt 1):185–199. [PubMed: 9490837]

Ang CW, et al. Massive and specific dysregulation of direct cortical input to the hippocampus in temporal lobe epilepsy. J Neurosci. 2006; 26:11850–11856. [PubMed: 17108158]

Bean BP. The action potential in mammalian central neurons. Nat Rev Neurosci. 2007; 8:451–465. [PubMed: 17514198]

Blasco-Ibanez JM, Freund TF. Synaptic input of horizontal interneurons in stratum oriens of the hippocampal CA1 subfield: structural basis of feed-back activation. Eur J Neurosci. 1995; 7:2170–2180. [PubMed: 8542073]

Buoni S, et al. SCN1A (2528delG) novel truncating mutation with benign outcome of severe myoclonic epilepsy of infancy. Neurology. 2006; 66:606–607. [PubMed: 16505326]

Carter BC, et al. Transient sodium current at subthreshold voltages: activation by EPSP waveforms. Neuron. 2012; 75:1081–1093. [PubMed: 22998875]

Catterall WA, et al. $Na_V1.1$ channels and epilepsy. J Physiol. 2010; 588:1849–1859. [PubMed: 20194124]

Cheah CS, et al. Specific deletion of $Na_V1.1$ sodium channels in inhibitory interneurons causes seizures and premature death in a mouse model of Dravet syndrome. Proc Natl Acad Sci U S A. 2012; 109:14646–14651. [PubMed: 22908258]

Claes L, et al. De novo SCN1A mutations are a major cause of severe myoclonic epilepsy of infancy. Hum Mutat. 2003; 21:615–621. [PubMed: 12754708]

Claes L, et al. De novo mutations in the sodium-channel gene SCN1A cause severe myoclonic epilepsy of infancy. Am J Hum Genet. 2001; 68:1327–1332. [PubMed: 11359211]

Claes LR, et al. The SCN1A variant database: a novel research and diagnostic tool. Hum Mutat. 2009; 30:E904–E920. [PubMed: 19585586]

Coulter DA, et al. Hippocampal microcircuit dynamics probed using optical imaging approaches. The Journal of Physiology. 2011; 589:1893–1903. [PubMed: 21224219]

Depienne C, et al. Mechanisms for variable expressivity of inherited SCN1A mutations causing Dravet syndrome. J Med Genet. 2010; 47:404–410. [PubMed: 20522430]

Dravet C, et al. Severe myoclonic epilepsy in infancy: Dravet syndrome. Adv Neurol. 2005; 95:71–102. [PubMed: 15508915]

Dutton SB, et al. Preferential inactivation of Scn1a in parvalbumin interneurons increases seizure susceptibility. Neurobiol Dis. 2012; 49C:211–220. [PubMed: 22926190]

Escayg A, Goldin AL. Sodium channel SCN1A and epilepsy: mutations and mechanisms. Epilepsia. 2010; 51:1650–1658. [PubMed: 20831750]

Estacion M, et al. A sodium channel mutation linked to epilepsy increases ramp and persistent current of $Na_V1.3$ and induces hyperexcitability in hippocampal neurons. Exp Neurol. 2010; 224:362–368. [PubMed: 20420834]

Frankel WN. Genetics of complex neurological disease: challenges and opportunities for modeling epilepsy in mice and rats. Trends Genet. 2009; 25:361–367. [PubMed: 19665252]

Fricker D, Miles R. EPSP amplification and the precision of spike timing in hippocampal neurons. Neuron. 2000; 28:559–569. [PubMed: 11144364]

Gambardella A, Marini C. Clinical spectrum of SCN1A mutations. Epilepsia. 2009; 50(Suppl 5):20–23. [PubMed: 19469841]

Genton P, et al. Dravet syndrome: the long-term outcome. Epilepsia. 2011; 52(Suppl 2):44–49. [PubMed: 21463279]

Goldman MS, et al. Global structure, robustness, and modulation of neuronal models. J Neurosci. 2001; 21:5229–5238. [PubMed: 11438598]

Gonzalez-Burgos G, Barrionuevo G. Voltage-gated sodium channels shape subthreshold EPSPs in layer 5 pyramidal neurons from rat prefrontal cortex. J Neurophysiol. 2001; 86:1671–1684. [PubMed: 11600631]

Guzzetta F. Cognitive and behavioral characteristics of children with Dravet syndrome: an overview. Epilepsia. 2011; 52(Suppl 2):35–38. [PubMed: 21463277]

Hajos N, Mody I. Synaptic communication among hippocampal interneurons: properties of spontaneous IPSCs in morphologically identified cells. J Neurosci. 1997; 17:8427–8442. [PubMed: 9334415]

Han S, et al. Autistic-like behaviour in Scn1a$^{+/-}$ mice and rescue by enhanced GABA-mediated neurotransmission. Nature. 2012a; 489:385–390. [PubMed: 22914087]

Han S, et al. $Na_V1.1$ channels are critical for intercellular communication in the suprachiasmatic nucleus and for normal circadian rhythms. Proc Natl Acad Sci U S A. 2012b; 109:E368–E377. [PubMed: 22223655]

Harkin LA, et al. The spectrum of SCN1A-related infantile epileptic encephalopathies. Brain. 2007; 130:843–852. [PubMed: 17347258]

Kalume F, et al. Sudden unexpected death in a mouse model of Dravet syndrome. J Clin Invest. 2013; 123:1798–1808. [PubMed: 23524966]

Kalume F, et al. Reduced sodium current in Purkinje neurons from $Na_V1.1$ mutant mice: implications for ataxia in severe myoclonic epilepsy in infancy. J Neurosci. 2007; 27:11065–11074. [PubMed: 17928448]

Klausberger T, et al. Brain-state- and cell-type-specific firing of hippocampal interneurons in vivo. Nature. 2003; 421:844–848. [PubMed: 12594513]

Klausberger T, Somogyi P. Neuronal diversity and temporal dynamics: the unity of hippocampal circuit operations. Science. 2008; 321:53–57. [PubMed: 18599766]

Li BM, et al. Autism in Dravet syndrome: prevalence, features, and relationship to the clinical characteristics of epilepsy and mental retardation. Epilepsy Behav. 2011; 21:291–295. [PubMed: 21620773]

Liautard C, et al. Hippocampal hyperexcitability and specific epileptiform activity in a mouse model of Dravet syndrome. Epilepsia. 2013; 54:1251–1261. [PubMed: 23663038]

Maccaferri G. Stratum oriens horizontal interneurone diversity and hippocampal network dynamics. J Physiol. 2005; 562:73–80. [PubMed: 15498801]

Maccaferri G, McBain CJ. Passive propagation of LTD to stratum oriens-alveus inhibitory neurons modulates the temporoammonic input to the hippocampal CA1 region. Neuron. 1995; 15:137–145. [PubMed: 7619518]

Maccaferri G, McBain CJ. The hyperpolarization-activated current (Ih) and its contribution to pacemaker activity in rat CA1 hippocampal stratum oriens-alveus interneurones. J Physiol. 1996; 497(Pt 1):119–130. [PubMed: 8951716]

Mahoney K, et al. Variable neurologic phenotype in a GEFS+ family with a novel mutation in SCN1A. Seizure. 2009; 18:492–497. [PubMed: 19464195]

Martina M, et al. Distal Initiation and Active Propagation of Action Potentials in Interneuron Dendrites. Science. 2000; 287:295–300. [PubMed: 10634782]

McKhann GM 2nd, et al. Mouse strain differences in kainic acid sensitivity, seizure behavior, mortality, and hippocampal pathology. Neuroscience. 2003; 122:551–561. [PubMed: 14614919]

Miller AR, et al. Mapping genetic modifiers of survival in a mouse model of Dravet syndrome. Genes, Brain and behavior. 2013 n/a-n/a.

Mistry AM, et al. Strain- and age-dependent hippocampal neuron sodium currents correlate with epilepsy severity in Dravet syndrome mice. Neurobiol Dis. 2014; 65:1–11. [PubMed: 24434335]

Nguyen PV. Comparative plasticity of brain synapses in inbred mouse strains. J Exp Biol. 2006; 209:2293–2303. [PubMed: 16731805]

Oakley JC, et al. Synergistic GABA-Enhancing Therapy against Seizures in a Mouse Model of Dravet Syndrome. J Pharmacol Exp Ther. 2013; 345:215–224. [PubMed: 23424217]

Oakley JC, et al. Temperature- and age-dependent seizures in a mouse model of severe myoclonic epilepsy in infancy. Proc Natl Acad Sci U S A. 2009; 106:3994–3999. [PubMed: 19234123]

Ogiwara I, et al. $Na_V1.1$ haploinsufficiency in excitatory neurons ameliorates seizure-associated sudden death in a mouse model of Dravet syndrome. Hum Mol Genet. 2013

Ogiwara I, et al. $Na_v1.1$ localizes to axons of parvalbumin-positive inhibitory interneurons: a circuit basis for epileptic seizures in mice carrying an Scn1a gene mutation. J Neurosci. 2007; 27:5903–5914. [PubMed: 17537961]

Pouille F, Scanziani M. Routing of spike series by dynamic circuits in the hippocampus. Nature. 2004; 429:717–723. [PubMed: 15170216]

Raman IM, Bean BP. Resurgent sodium current and action potential formation in dissociated cerebellar Purkinje neurons. J Neurosci. 1997; 17:4517–4526. [PubMed: 9169512]

Reid CA, et al. Reduced dendritic arborization and hyperexcitability of pyramidal neurons in a Scn1b-based model of Dravet syndrome. Brain. 2014; 137:1701–1715. [PubMed: 24747835]

Rotaru DC, et al. Dopamine D1 receptor activation regulates sodium channel-dependent EPSP amplification in rat prefrontal cortex pyramidal neurons. J Physiol. 2007; 581:981–1000. [PubMed: 17395630]

Salazar BC, et al. Multiple open channel states revealed by lidocaine and QX-314 on rat brain voltage-dependent sodium channels. J Gen Physiol. 1996; 107:743–754. [PubMed: 8783074]

Schauwecker PE. The relevance of individual genetic background and its role in animal models of epilepsy. Epilepsy Res. 2011; 97:1–11. [PubMed: 22001434]

Scheffer IE, et al. Dravet syndrome or genetic (generalized) epilepsy with febrile seizures plus? Brain Dev. 2009; 31:394–400. [PubMed: 19203856]

Schimanski LA, Nguyen PV. Multidisciplinary approaches for investigating the mechanisms of hippocampus-dependent memory: a focus on inbred mouse strains. Neurosci Biobehav Rev. 2004; 28:463–483. [PubMed: 15465135]

Schwindt PC, Crill WE. Amplification of synaptic current by persistent sodium conductance in apical dendrite of neocortical neurons. J Neurophysiol. 1995; 74:2220–2224. [PubMed: 8592214]

Stuart G, Sakmann B. Amplification of EPSPs by axosomatic sodium channels in neocortical pyramidal neurons. Neuron. 1995; 15:1065–1076. [PubMed: 7576650]

Suls A, et al. Four generations of epilepsy caused by an inherited microdeletion of the SCN1A gene. Neurology. 2010; 75:72–76. [PubMed: 20484682]

Swensen AM, Bean BP. Robustness of burst firing in dissociated purkinje neurons with acute or long-term reductions in sodium conductance. J Neurosci. 2005; 25:3509–3520. [PubMed: 15814781]

Tai C, et al. Impaired excitability of somatostatin- and parvalbumin-expressing cortical interneurons in a mouse model of Dravet syndrome. Proc Natl Acad Sci U S A. 2014; 111:E3139–E3148. [PubMed: 25024183]

Tort AB, et al. On the formation of gamma-coherent cell assemblies by oriens lacunosum-moleculare interneurons in the hippocampus. Proc Natl Acad Sci U S A. 2007; 104:13490–13495. [PubMed: 17679692]

Verbeek NE, et al. Prevalence of SCN1A Related Dravet Syndrome among Children Reported with Seizures following Vaccination: A Population-Based Ten-Year Cohort Study. PLoS ONE. 2013; 8:e65758. [PubMed: 23762420]

Vervaeke K, et al. Contrasting effects of the persistent Na^+ current on neuronal excitability and spike timing. Neuron. 2006; 49:257–270. [PubMed: 16423699]

Weiss LA, et al. Sodium channels SCN1A, SCN2A and SCN3A in familial autism. Mol Psychiatry. 2003; 8:186–194. [PubMed: 12610651]

Westenbroek RE, et al. Differential subcellular localization of the RI and RII Na+ channel subtypes in central neurons. Neuron. 1989; 3:695–704. [PubMed: 2561976]

Yu FH, et al. Reduced sodium current in GABAergic interneurons in a mouse model of severe myoclonic epilepsy in infancy. Nat Neurosci. 2006; 9:1142–1149. [PubMed: 16921370]

HIGHLIGHTS

- DS ($Na_V1.1^{+/-}$) mice in 129/SvJ genetic background have milder epilepsy than C57BL/6
- DS interneurons have higher threshold and rheobase and decreased synaptic boosting
- Excitability of DS interneurons from 129/SvJ mice is better maintained than C57BL/6

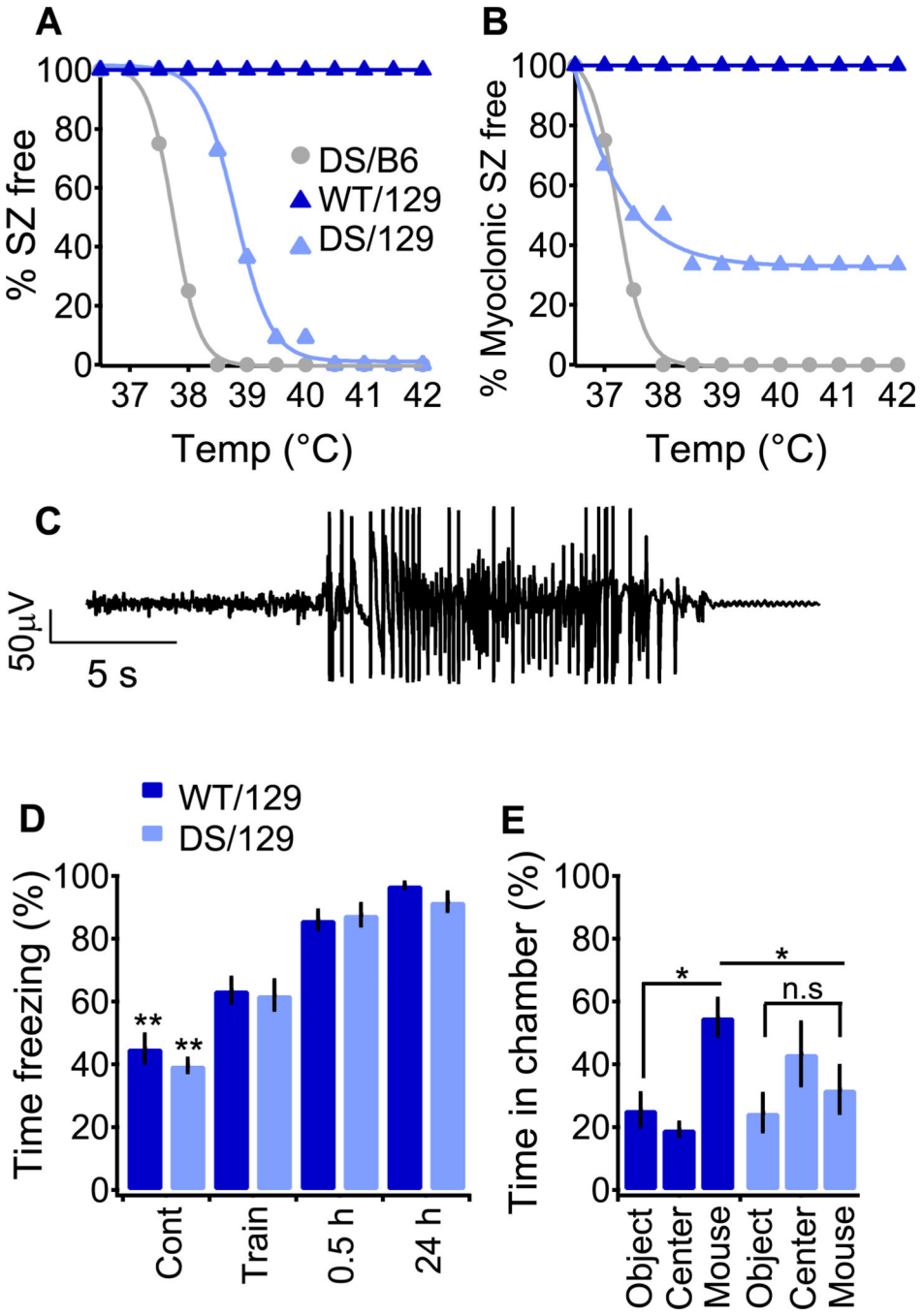

Fig. 1. Characterization of the epileptic phenotype of DS/129 mice

(A and B) Induction of seizures by increasing body core temperature. (A) Percentage of P21 mice remaining free of behavioral seizures (SZ) versus body core temperature, fitted with a sigmoid (line). WT mice of either strain do not have seizures at the tested temperatures. DS/129, n=11, DS/B6 n=4. (B) Percentage of mice remaining free of behavioral myoclonic seizures. (C) Representative intracranial EEG activity of DS/129 at P28. The depicted seizure was recorded at 40 °C. (D) Contextual fear conditioning test. WT/129 and DS/129 display similar freezing behavior during training and when reintroduced to the chamber 0.5

and 24 h later. n=14 for each genotype. (E) Three-chamber experiment. WT/129 mice spend more time in the chamber housing a stranger mouse (mouse) than the chamber housing an empty cage (object) or in the connecting chamber (center). DS/129 mice have no preference for either chamber. n=10 for each genotype.

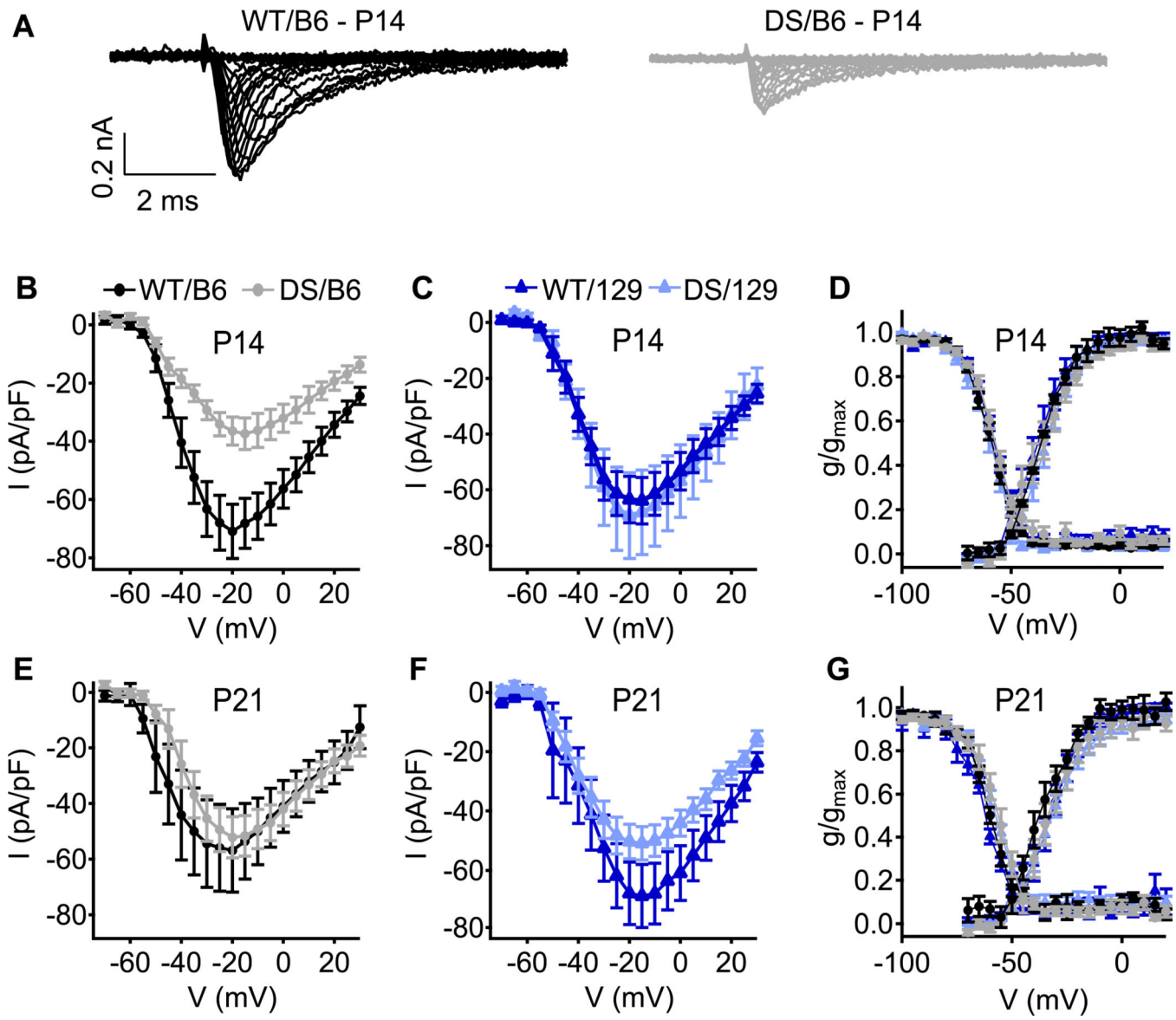

Fig. 2. Sodium currents of WT and DS in acutely dissociated hippocampal inhibitory neurons

(A) Representative sets of sodium current traces from inhibitory neurons of WT/B6 and DS/B6 at P14. (B, C) Current–voltage relationships of whole-cell sodium currents from B6 (B) and 129 (C) interneurons at P14. (D) Voltage dependence of activation (right curves) and steady-state inactivation (left curves) of sodium currents at P14 (E, F) Current–voltage relationships of whole-cell sodium currents from B6 (E) and 129 (F) interneurons at P21. (G) Voltage dependence of activation (right curves) and steady-state inactivation (left curves) of sodium currents at P21. n=11–16.

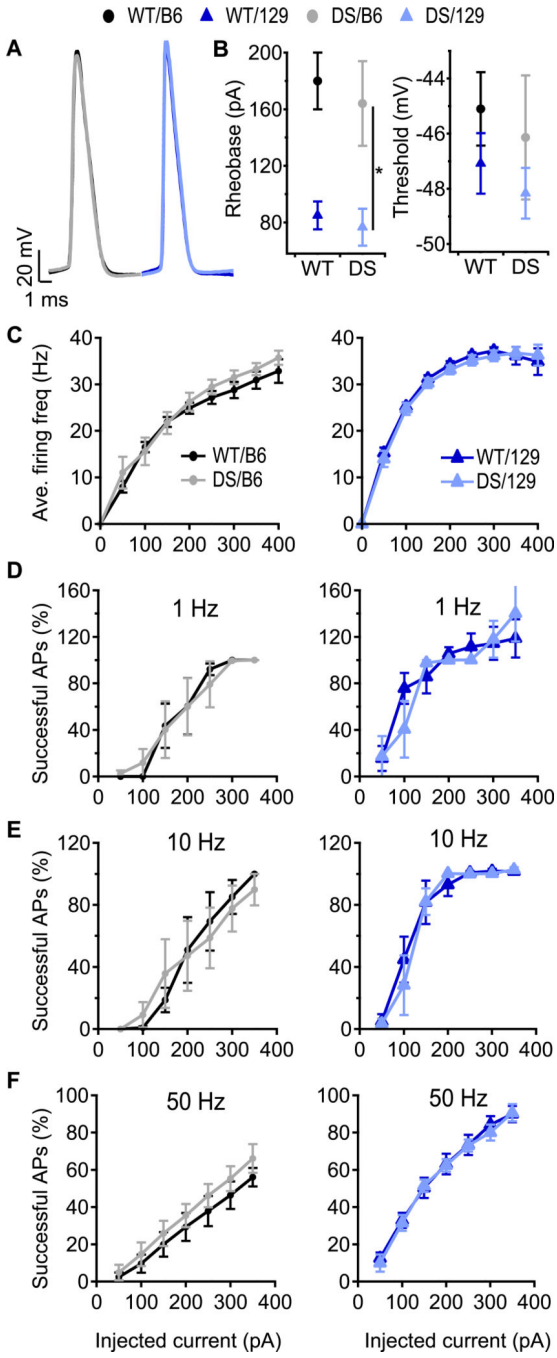

Fig. 3. Firing properties of CA1 pyramidal neurons are not changed by the DS mutation

(A) Representative APs of CA1 pyramidal neurons induced by 10 ms depolarizing current pulses through the patch pipette at rheobase. (B) Mean AP rheobase and threshold. (C) Average firing frequency of CA1 pyramidal cells in response to 1 s depolarizing current injection at the indicated intensity. n=5–8. (D–F) Percent successful APs in pyramidal neurons in response to 10 ms, depolarizing current pulses at 1 Hz (D), 10 Hz (E) and 50 Hz (F). 100% indicates one successful AP in every trial; values > 100% indicate that 2 APs were evoked during the 10 ms depolarization. n=5–7.

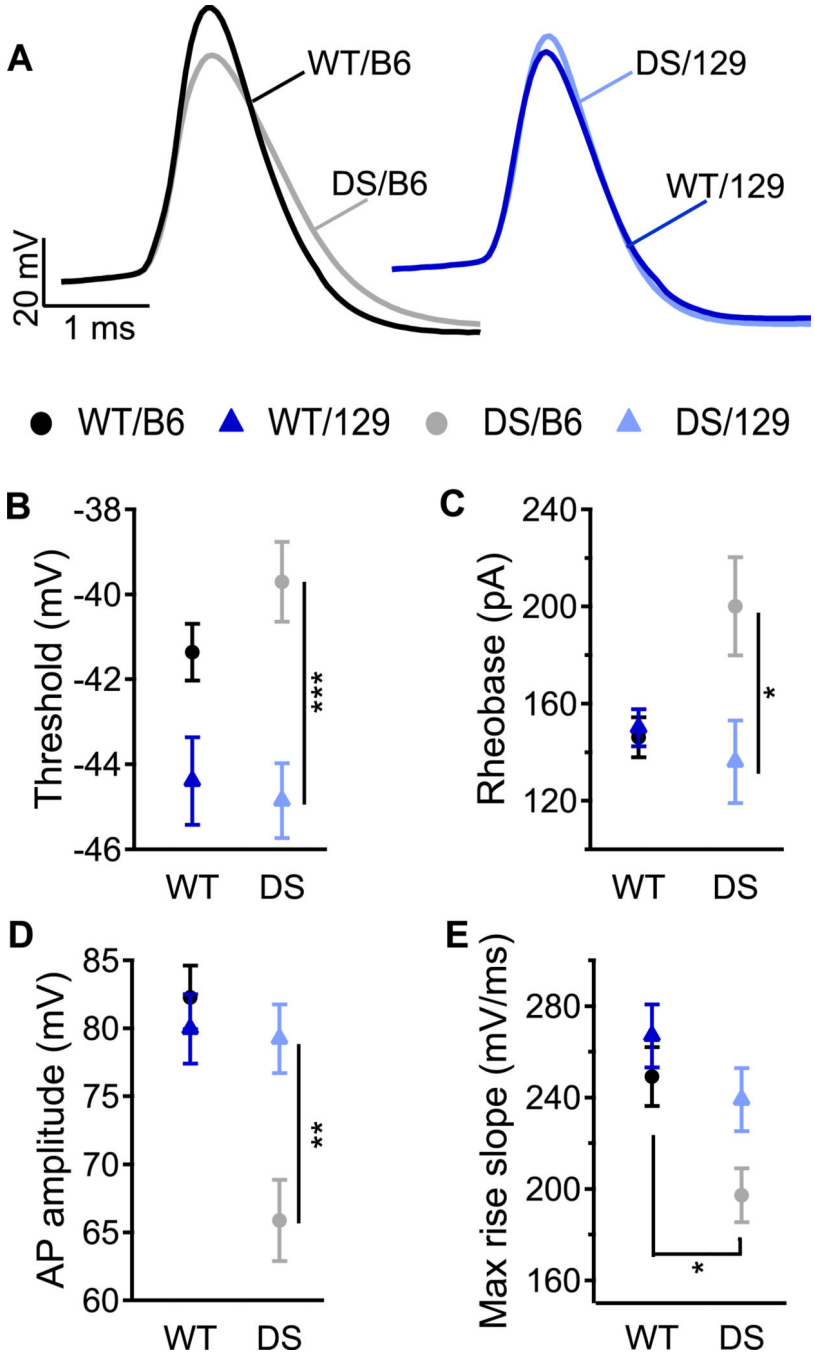

Fig. 4. Lesser excitability of *SO* interneurons of DS/B6 mice relative to DS/129

(A) Representative APs of *SO* interneurons induced by 10 ms depolarizing current pulses through the patch pipette at rheobase. (B–E) Mean AP threshold (B), rheobase (C), AP amplitude (D) and max rise slope (E). n=11–13.

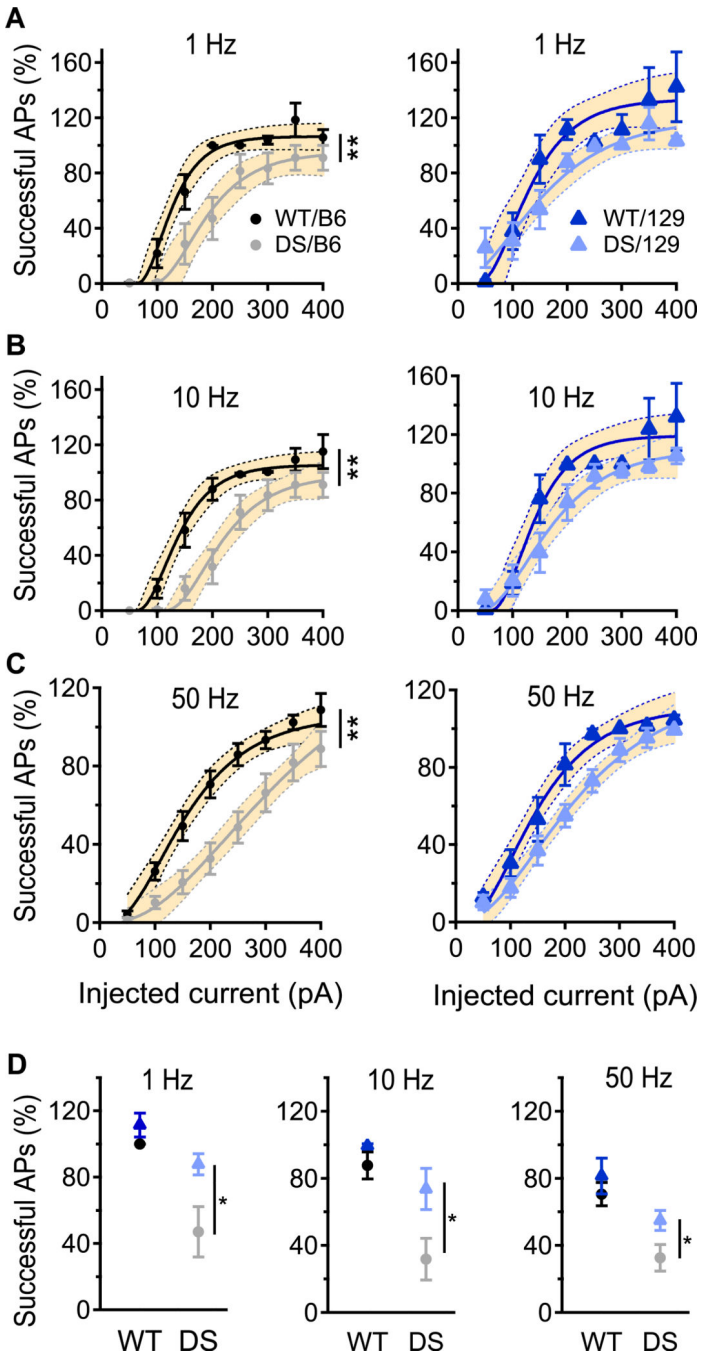

Fig. 5. Greater impairment of *SO* interneuron firing in DS/B6 than in DS/129

(A – C) Percent of 10 ms depolarizing current pulses at 1 Hz (A), 10 Hz (B) and 50 Hz (C) that produced successful APs in *SO* interneurons. 100% indicates one successful AP in every trial; values > 100% indicate that 2 APs were evoked during the 10 ms depolarization. Solid lines are fits of an empirical equation $(A[1\text{-}\exp(-I \times D)])^3$ to the data where A is the amplitude, I is the current and D is a constant. The shaded area is the 95% confidence interval of the fit, and the non-overlapping areas are statistically significant ($p<0.05$). Statistical significance was also calculated using area under the curve. DS/B6 fire less AP

compare to WT/B6 at 1 Hz, 10 Hz and 50 Hz, $p<0.01$. Firing of 129/DS was similar to that of 129/WT at tested frequencies $p>0.05$. (D) Percent successful APs in response to the 200 pA current pulses. n= 8–11.

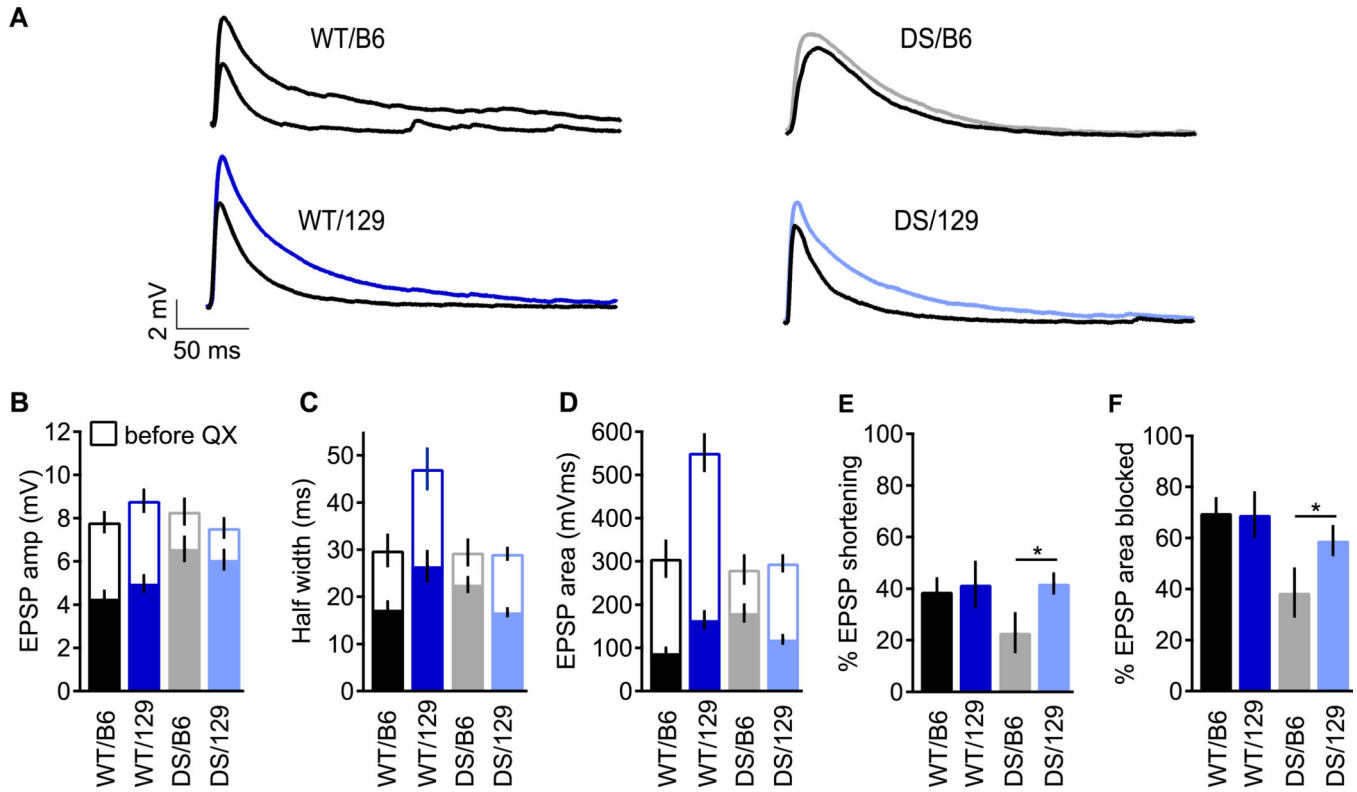

Fig. 6. Sodium channels contribute less to amplification of subthreshold EPSPs in DS/B6

EPSPs were generated by retrograde stimulation of CA1 neurons using a stimulating electrode in the alveus. Stimulus intensity was adjusted to give an EPSP amplitude of approximately 8 mV. (A) Representative EPSP traces before (colored) and after (black) sodium channel block by QX-314 (5–10 μM). (B–D) EPSP parameters before (empty bars) and after (solid bars) block with QX-314. EPSP amplitude (B), EPSP duration (C) and EPSP area (D). Percent sodium channel contribution to EPSP duration (E) and area (F). n=6–10.

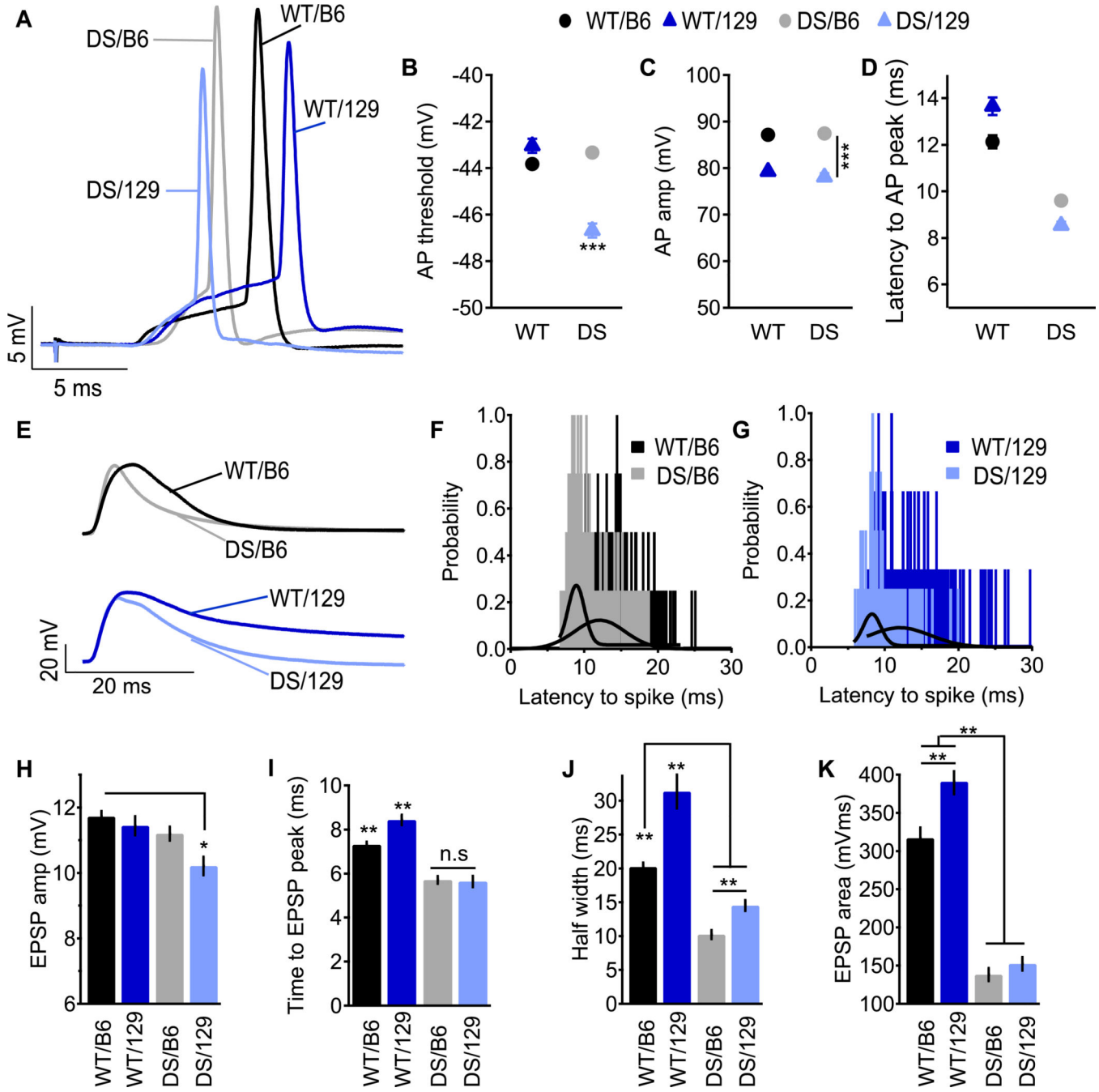

Fig. 7. Properties of synaptically evoked APs and near-threshold EPSPs in *SO* Interneurons

Stimulating electrode was placed in the alveus and the stimulation strength was set to produce firing probability of 50% during trains of 10 stimuli at 1 Hz. Representative APs (A) and EPSPs (E). (B–D) Parameters of synaptically evoked APs. Mean AP threshold (B), amplitude (C) and the latency to spike (D). (F–G) Histogram and Gaussian fit (solid line) of the latency to AP. (H–J) Parameters of near-threshold EPSP. Mean EPSP amplitude (H), time to peak (I), duration (J) and area (K). n=9–20.

Table 1

Action potential parameters of CA1 pyramidal neurons and CA1 Stratum Oriens interneurons

A. AP parameters CA1 pyramidal neurons						
	Rheo (pA)	**Threshold**	**AP amplitude (mV)**	**AP half width (ms)**	**max rise slope (mV/ms)**	**n**
WT/129	85.00 ± 9.82 *a*	−47.08 ± 1.10	113.06 ± 1.51 *b*	1.32 ± 0.02 *b*	556.94 ± 18.60	8
DS/129	76.67 ± 13.08 *a*	−48.16 ± 0.92	109.87 ± 1.75	1.36 ± 0.04	488.15 ± 33.03	6
WT/B6	180.00 ± 20.00	−45.10 ± 1.33	103.28 ± 3.77	1.48 ± 0.04	406.88 ± 33.61	6
DS/B6	164.00 ± 29.93	−46.14 ± 2.25	108.60 ± 1.87	1.37 ± 0.03	507.22 ± 71.15	5

B. AP parameters CA1 *Stratum Oriens* interneurons						
	Rheo (pA)	**Threshold**	**AP amplitude (mV)**	**AP half width (ms)**	**max rise slope (mV/ms)**	**n**
WT/129	150.00 ± 7.59	−44.39 ± 1.03	79.96 ± 2.56	0.78 ± 0.08	266.85 ± 13.82	12
DS/129	140.00 ± 15.95	−44.86 ± 0.88	79.22 ± 2.53	0.74 ± 0.05	239.05 ± 13.82	10
WT/B6	146.15 ± 8.28	−41.36 ± 0.67	82.28 ± 2.34	0.84 ± 0.04	249.18 ± 12.86	13
DS/B6	200.00 ± 20.25 *c*	−39.71 ± 0.94 *d*	65.87 ± 2.99	0.84 ± 0.05	197.22 ± 11.82 *e*	13

a $p<0.05$ vs WT/B6 and DS/B6

b $p<0.05$ vs WT/B6

c $p<0.05$ vs DS/129

d $p<0.05$ vs WT/129 and DS/129

e $p<0.05$ vs WT/129 and WT/B6